International Journal of Development Mathematics Vol 3 Issue 2 Page No. 043 - 55

INTERNATIONAL JOURNAL OF DEVELOPMENT MATHEMATICS

ISSN: 3026-8656 (Print) | 3026-8699 (Online)

journal homepage: https://ijdm.org.ng/index.php/Journals

Effects of Heat Sink and Heat Absorption on Casson Fluid Flow in a Vertical Channel

Abdullahi Hussaini[a], Emmanuel Omokhuale[b], Abdullahi A. Sifawa[c] and Salisu Saleh[d*]

[a,c]Department of Mathematics, Sokoto State University, Nigeria
[b]Department of Mathematical Sciences, Federal University Gusau, Nigeria
[d]Department of Mathematics, Zamfara State University Talata Mafara, Nigeria

ARTICLE INFO

Article history:
Received 10 March 2026
Received in revised form 20 May 2026
Accepted 30 May 2026

Keywords:
Heat Sink, Heat Absorption, Casson Fluid, Vertical Channel, Magnetohydrodynamics, Finite Difference Method

MSC 2020 Subject classification:
80A20

ABSTRACT

This study examines the effects of heat sink and heat absorption on Casson fluid flow in a vertical channel. The flow is governed by partial differential equations (PDEs). Using suitable dimensionless variables, these PDEs were transformed into non-dimensional form. The implicit finite difference method (IFDM) was employed to obtain approximate solutions for the velocity, temperature, and concentration distributions of the fluid. The effects of physical parameters associated with the fluid flow, such as magnetohydrodynamics, thermal radiation, chemical reaction, heat generation, and permeability of the porous medium, on unsteady free convective heat and mass transfer over a vertical porous plate were investigated. Key parameters such as the Hartmann number, Darcy number, and thermal Grashof number are essential for applications in geothermal systems and chemical processing. Numerical solutions of the governing equations reveal that a higher Hartmann number decreases fluid velocity due to the Lorentz force, whereas an increased Darcy number enhances velocity due to greater permeability. Additionally, thermal radiation and heat sources raise temperature profiles, while buoyancy forces increase velocity distributions. The effects of suction on the boundary layer thickness are also analyzed, and a higher chemical reaction parameter reduces concentration. The study concludes that suction improves heat and mass transfer rates, while stronger magnetic fields may elevate wall shear stress, offering insights for optimizing industrial processes involving electrically conducting fluids in porous media under magnetic influence.

1. Introduction

A fluid is a substance that continuously deforms under the application of shear stress, and its flow behavior plays a crucial role in numerous engineering and industrial processes. Fluids are generally classified as Newtonian and non-Newtonian based on the relationship between shear stress and strain rate. Unlike Newtonian fluids, non-Newtonian fluids exhibit variable viscosity depending on the applied stress, making their flow characteristics more complex and highly relevant in practical applications.

Among non-Newtonian fluids, the Casson fluid model has received considerable attention due to its ability to accurately describe the rheological behavior of materials such as blood, honey, jelly, and various industrial suspensions. Casson fluids are characterized by a yield stress, below which the fluid behaves like a solid and above which it flows as a viscous fluid. This unique property makes the model suitable for analyzing a wide range of biological and industrial processes. Consequently, numerous studies have explored the influence of different physical parameters on Casson fluid flow, particularly in the context of heat and mass transfer (Kumar et al., 2023; Reddy & Janardhan, 2017).

The interaction between magnetic fields and electrically conducting fluids gives rise to magnetohydrodynamic (MHD) flow, which has significant applications in systems such as MHD generators, nuclear reactor cooling, and metallurgical

* Corresponding author. Tel.: +2347068559610
E-mail address: salehsalisuagp@gmail.com (Salisu S.)
https://doi.org/10.62054/ijdm/0302.03

processes. The presence of a magnetic field introduces the Lorentz force, which acts as a resistive force and significantly alters the velocity and thermal profiles of the fluid. As a result, the study of MHD Casson fluid flow has become increasingly important in the design and optimization of modern engineering systems (Mangamma et al., 2024).

Thermal radiation plays a vital role in high-temperature environments, including combustion systems, energy devices, and aerospace applications, where it contributes significantly to overall heat transfer. Incorporating radiative effects into fluid flow analysis enhances the accuracy of temperature predictions and heat transfer rates. Similarly, heat source and heat sink mechanisms are essential in controlling the thermal behavior of fluid systems. Heat generation increases thermal energy within the fluid, whereas heat absorption reduces it, thereby influencing both temperature distribution and flow characteristics. These effects are particularly important in applications such as cooling technologies, energy storage systems, and chemical processing industries (Ramzan et al., 2021).

Another important factor in thermal transport is viscous dissipation, which represents the conversion of kinetic energy into thermal energy due to fluid friction. This effect becomes significant in flows with large velocity gradients and contributes to an increase in fluid temperature. The combined influence of viscous dissipation, thermal radiation, magnetic fields, and heat source/sink mechanisms is therefore essential for understanding complex heat and mass transfer processes in non-Newtonian fluids.

Over the years, several researchers have investigated MHD Casson fluid flow under various physical conditions. Early studies, such as Das et al. (2015), examined unsteady hydromagnetic Casson fluid flow over vertical plates with thermal radiation and chemical reaction, emphasizing the importance of thermal effects in boundary layer development. Subsequent works have extended these analyses to more complex scenarios. For instance, Anwar et al. (2021) analyzed unsteady MHD Casson fluid flow with suction/injection and thermal radiation, while Awais et al. (2021) studied the combined effects of heat generation/absorption and magnetic fields in porous media. More recent studies, including Bathmanaban et al. (2024) and Kumar et al. (2025), have investigated convective and time-dependent Casson fluid flows with heat transfer effects, demonstrating the strong coupling between thermal and momentum transport processes.

In addition, viscous dissipation and thermal radiation have been widely studied due to their significant impact on temperature distribution and energy transport. Reddy et al. (2018), Akbar et al. (2022), and Ilango and Lakshminarayana (2024) analyzed the role of viscous dissipation in MHD Casson fluid flow, reporting an increase in fluid temperature due to energy conversion. Similarly, studies by Mythili and Sivaraj (2016), Vinod et al. (2025), and Nisar et al. (2025) highlighted the influence of heat source/sink mechanisms on flow behavior. Suction and injection effects have also been shown to play a critical role in controlling boundary layer thickness and enhancing heat transfer efficiency (Abo-Dahab et al., 2021; Rehman et al., 2024; Nihaal et al., 2025).

Despite these extensive contributions, most existing studies primarily focus on flow over vertical plates rather than flow within vertical channels, which are more representative of practical engineering systems. Furthermore, limited attention has been given to the combined effects of heat sink (heat absorption) and viscous dissipation in MHD Casson fluid flow through porous vertical channels. The simultaneous interaction of key parameters such as magnetic field, thermal radiation, porous medium permeability, and buoyancy forces within a unified channel flow model also remains insufficiently explored. This lack of comprehensive analysis restricts accurate prediction and optimization of heat and mass transfer processes in real-world applications.

Therefore, the present study aims to address this gap by developing a numerical model to investigate viscous dissipative MHD Casson fluid flow in a vertical porous channel under the influence of thermal radiation and heat source/sink effects. Particular emphasis is placed on analyzing velocity, temperature, and concentration distributions, as well as important engineering parameters such as skin friction, Nusselt number, and Sherwood number.

2. Method

2.1 Problem Formulation

In Figure 2.1, the flow is being confined to $y' > 0$, where y' the coordinate is measured in the normal direction to the plate and the $x' -$ axis is taken along the plane in the upward direction. Initially, at time $t' \leq 0$, both the fluid and the plate are at rest at a uniform temperature T'_{∞} and surface concentration is assumed to be C'_{∞}. At time $t' > 0$, the plate temperature and surface concentration are lowered below the ambient temperature and ambient concentration, respectively. The fluid is permeated by uniform transverse magnetic field B_0 applied parallel in the $y' -$ axis direction.

The effects of viscous dissipation are considered, while the induced magnetic and electric fields are neglected because magnetic Reynolds number is very small for liquid metals and partially ionized fluid. The effects of viscous dissipation, induced magnetic and electrical field are not neglected.

Following Kataria and Patel (2019) and Usman *et al.* (2022), under the above assumptions and taking into account the Boussinesq's approximation, the governing equations are given below:

The constitutive equation for Casson fluid can be expressed as follows:

$$\tau_{ij} = \begin{cases} 2\left(\mu_B + \frac{P_y}{\sqrt{2\pi}}\right) e_{ij} \ \ when\ \pi > \pi_c, \\ 2\left(\mu_B + \frac{P_y}{\sqrt{2\pi}}\right) e_{ij} \ \ when\ \pi < \pi_c. \end{cases} \tag{2.1}$$

In the equation (2.1), $\pi = e_{ij}e_{ij}$ and e_{ij} $-$indicates $(i,j)^{th}$ the rate of deformity component, $\pi_c -$ indicates the critical stress based on the non-Newtonian model, $\pi -$ indicate product of self deformation rate, and $P_y -$ indicate fluid's yield stress.

Following Reddy *et al.* (2024), the governing equations of this model will be written in dimensional form as follow:

The basic assumptions of the present model are:

1. A continuous magnetic field $B = (B_0 cos\gamma, B_0 sin\gamma, 0)$ is enforced in $y' -$ direction with an angle γ with $y' > 0$;
2. The magnetic Reynolds number estimated to be small; hence the importance of the magnetic field infused by flow impetus is ignored;
3. There is no externally sanctioned electric field, so that the response polarization is overlooked;
4. The fluid flow is originated by the plate impulsive motion in $x' -$ direction and due to the pores in the plate surface there is no constant flow in the $y' -$ direction, hence the velocity vector is given by $q = (u', v_0, 0)$.

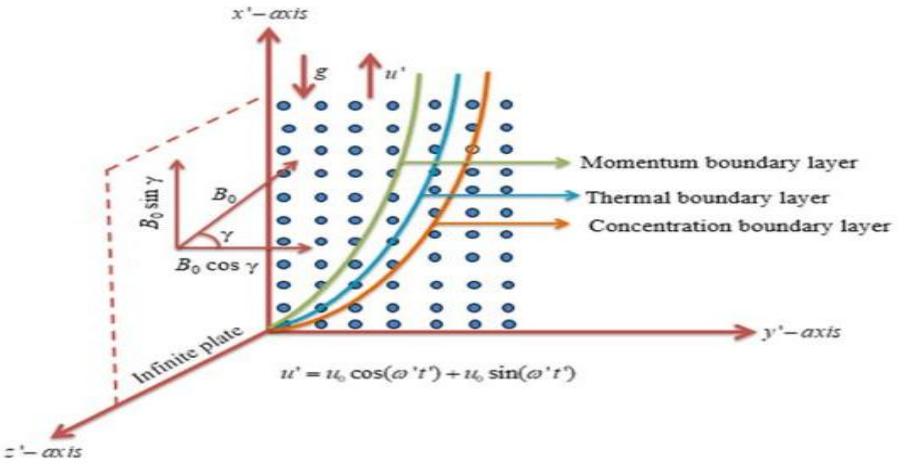

Figure 3.1: Schematic Diagram

Continuity Equation

$$\frac{\partial v'}{\partial y'} = 0 \tag{2.2}$$

Momentum Equation

$$\rho\left(\frac{\partial u'}{\partial t'} + v_0\frac{\partial u'}{\partial y'}\right) = \mu\left(\frac{1}{\gamma}+1\right)\frac{\partial^2 u'}{\partial y'^2} - \sigma B_0^2 u' - \mu\left(\frac{1}{\gamma}+1\right)\frac{u'}{K'} + \rho g[\beta^T(T'-T_0') + \beta^C(C'-C_0')] \tag{2.3}$$

Energy Equation:

$$\rho C_p\left(\frac{\partial T'}{\partial t'} + v_0\frac{\partial T'}{\partial y'}\right) = k\frac{\partial^2 T'}{\partial y'^2} - Q_0(T'-T_0') - \frac{\partial q_r}{\partial y'} \tag{2.4}$$

Mass Equation:

$$\frac{\partial C'}{\partial t'} + v_0 \frac{\partial C'}{\partial y'} = D_m \frac{\partial^2 C'}{\partial y'^2} - k_c'(C' - C_0') \tag{2.5}$$

with the following initial and boundary conditions:

$$\left.\begin{array}{l} t' \le 0, u' = 0, T' = T_0', C' = C_0' \ for\, all\ y' \\ t' > 0, u' = 0, T' = T_w', C' = C_w' \ at\ y' = 0 \\ \qquad u' = 0, T' = T_0', C' = C_0' \, at\ y' = h \end{array}\right\} \tag{2.6}$$

The radiative heat flux term by using Rosseland approximation is given by

$$q_r = -\frac{4\sigma}{3k_1}\frac{\partial T^4}{\partial y} \tag{2.7}$$

here, k_1 and σ_s represent respectively, the mean absorptive and Stefan–Boltzmann constant. We presume that the temperature changes inside the flow allow the expansion of T^4 by using Taylor series expansion about T_∞, neglecting higher order terms (i.e., from 2nd order terms), bring about;

$$T'^4 \cong 4T'^3_0 T' - T'^4_o \tag{2.8}$$

On introducing the following non-dimensional quantities

$$y = \frac{y'}{h}, u = \frac{u'}{u_0};\ \ t = \frac{t'\upsilon}{\mathrm{h}^2}, \theta = \frac{T' - T_0'}{T_w' - T_0'}, C = \frac{C' - C_0'}{C_w' - C_0'} \tag{2.9}$$

Using (2.2), (2.7) to (2.9), equations (2.3) to (2.5) are transformed into the following:

$$\frac{\partial u}{\partial t} + S\frac{\partial u}{\partial y} = \left(\frac{1}{\gamma} + 1\right)\frac{\partial^2 u}{\partial y^2} - M^2 u - \left(\frac{1}{\gamma} + 1\right)\frac{u}{Da} + Gr\theta + GcC \tag{2.10}$$

$$\frac{\partial \theta}{\partial t} + S\frac{\partial \theta}{\partial y} = \frac{1}{Pr}\frac{\partial^2 \theta}{\partial y^2} + H_T\theta + \frac{4N_r}{3Pr}\frac{\partial^2 \theta}{\partial y^2} \tag{2.11}$$

$$\frac{\partial C}{\partial t} + S\frac{\partial C}{\partial y} = \frac{1}{Sc}\frac{\partial^2 C}{\partial y^2} - K_c C \tag{2.12}$$

With the following boundary conditions:

$$\left.\begin{array}{l} t \le , u = 0, \theta = 0, C = 0\ for\ all\ y \\ t > 0 \begin{cases} u = 0, \theta = 1, C = 1\ at\ y = 0 \\ u = 0, \theta = 0, C = 0\ at\ y = 1 \end{cases} \end{array}\right. \tag{2.13}$$

where Gr is the thermal Grashof number, Gc is the mass Grashof number, Sc is the Schmidt number, Pr is the Prandtl number, M is the magnetic parameter, K is the permeability parameter, S is the injection parameter, *Kc* is chemical reaction parameter, Nr is radiation parameter, *Ht* is heat source/sink parameter, *Da* is Darcy number, *V* Kinematic Viscosity, u is Velocity, θ is temperature, C is concentration, t is Time,

$$M^2 = \frac{\sigma B_0^2 h^2}{\rho v}, Da = \frac{k'}{h^2}, Gr = \frac{g\beta^T(T_w' - T_0')h^2}{\upsilon u_0}, Gc = \frac{g\beta^C(C_w' - C_0')h^2}{\upsilon u_0}, S = \frac{v_0 h}{v}, \alpha = \frac{K}{\rho C_p}, \tag{2.13}$$

$$Pr = \frac{v}{\alpha}, H_T = \frac{Q_0 h^2}{\rho C_p v}, N_r = \frac{4\sigma_s T_0^3}{3Kk_1}, Sc = \frac{v}{Dm}, K_c = \frac{k_c' h^2}{v}.$$

Equations (2.10) to (2.12) are now approximated by implicit finite difference schemes of Crank – Nicolson type. The finite difference approximations of these equations are as follows:

$$\left(\frac{u_{i,j+1} - u_{i,j}}{\Delta t} + S\frac{u_{i+1,j} - u_{i,j}}{\Delta y}\right) = \left(\frac{1}{\gamma} + 1\right)\left[\frac{u_{i+1,j} + u_{i-1,j} - 2u_{i,j} + u_{i+1,j+1} + u_{i-1,j+1} - 2u_{i,j+1}}{2(\Delta y)^2}\right]$$

$$+ \frac{Gr}{2}\left(\theta_{i,j+1} + \theta_{i,j}\right) + \frac{Gc}{2}\left(C_{i,j+1} + C_{i,j}\right) - \frac{M^2}{2}\left(u_{i,j+1} + u_{i,j}\right) - \frac{1}{2Da}\left(\frac{1}{\gamma} + 1\right)\left(u_{i,j+1} + u_{i,j}\right) \tag{2.14}$$

$$\left(\frac{\theta_{i,j+1} - \theta_{i,j}}{\Delta t} + S\frac{\theta_{i+1,j} - \theta_{i,j}}{\Delta y}\right) = \frac{1}{\mathrm{Pr}} \cdot \left[1 + \frac{4N_r}{3}\right]\left[\frac{\theta_{i+1,j} - \theta_{i-1,j} - 2\theta_{i,j} + \theta_{i+1,j+1} + \theta_{i-1,j+1} - 2\theta_{i,j+1}}{2(\Delta y)^2}\right]$$

$$+\frac{H_T}{2}\left(\theta_{i,j+1}+\theta_{i,j}\right) \tag{2.15}$$

$$\left(\frac{C_{i,j+1}-C_{i,j}}{\Delta t}+S\frac{C_{i+1,j}-C_{i,j}}{\Delta y}\right)=\frac{1}{Sc}\left[\frac{C_{i+1,j}-C_{i-1,j}-2C_{i,j}+C_{i+1,j+1}+C_{i-1,j+1}-2C_{i,j+1}}{2(\Delta y)^2}\right]$$

$$-\frac{K_c}{2}\left(C_{i,j+1}+C_{i,j}\right) \tag{2.16}$$

The initial and boundary conditions become

$$\begin{aligned} &u_{i,0}=0,\theta=0,C_{i,0}=0 \text{ for all i except } i=0\\ &u_{l,0}=0,\theta_{l,0}=1,C_{l,0}=1\\ &u_{l,0}=0,\theta_{l,0}=0,C_{l,0}=0 \end{aligned} \tag{2.17}$$

where l corresponds to 1. The suffix i corresponds to y and j is equals to t. consequently, $\Delta t=t_{j+1}-t_j$ and $\Delta y=y_{i+1}-y_i$.

In order to access the effects of parameters on the flow variables namely; Casson parameter, thermal Grashof number, mass Grashof number, Schmidt number, Prandtl number, magnetic parameter, Darcy parameter, injection parameter, heat absorption parameter, radiation parameter, chemical reaction parameter on the velocity, temperature and concentration, and have grips of the physical problem, the unsteady coupled non-linear partial differential equations (12) – (14) with boundary conditions (15). Computations were performed using MATLAB with the following values for Gr =0.5 Gc = 0.05 M^2 = 0, $\gamma=0.5$, *Pr* = 0.71, *Sc* = 0.3, S = 0.1, K_c = 0.5, R = 0.1, Da = 0.05, t = 0.05, s = -2 N=0 except where they are varied. A step size of $\Delta t=0.01$, Δy = 0.25 is used for the interval $y_{\min}$ = 0 to $y_{\max}$ = 1 for a desired accuracy and a convergence criterion of 10^{-6} is satisfied for various parameters.

3. Results and Discussion

For the values of C, θ, u at time t, the values at a time $t+\Delta t$ gotten for $i=1,2,...,l-1$ in (2.16) which results in a tri-diagonal system of equations in unknown values of C. Similarly, calculating θ and u from (2.15) and (2.14), respectively.

4.1 Results

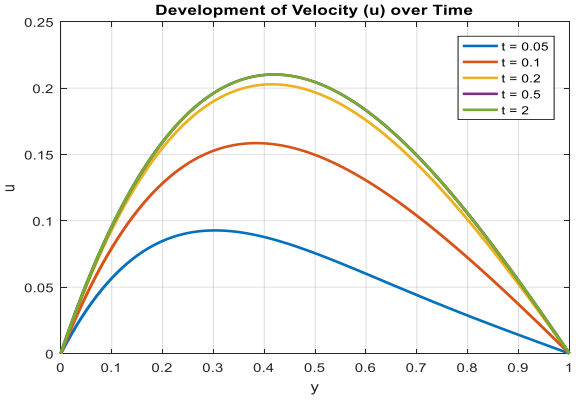

Figure 4.1: Velocity for different values of *t*

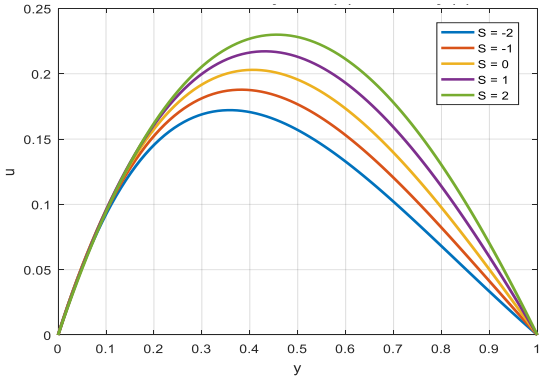

Figure 4.2: Velocity for different values of *S*

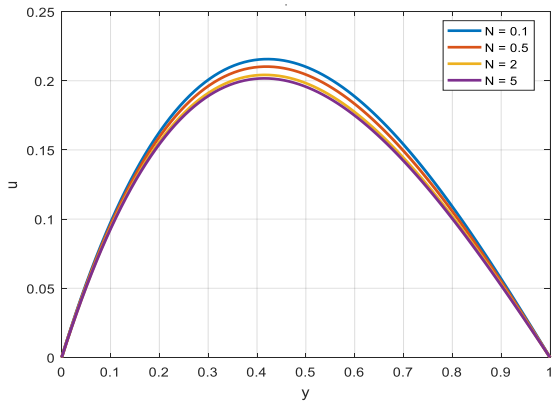

Figure 4.3: Velocity for different values of N

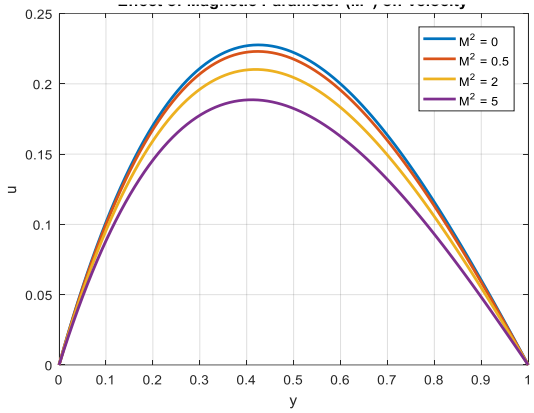

Figure 4.4:Velocity for different values of M^2

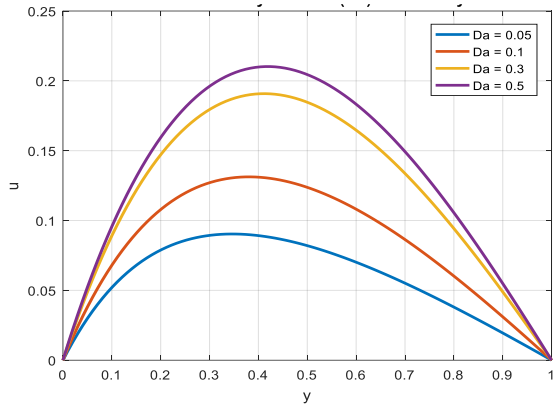

Figure 4.5: Velocity for different values of Da

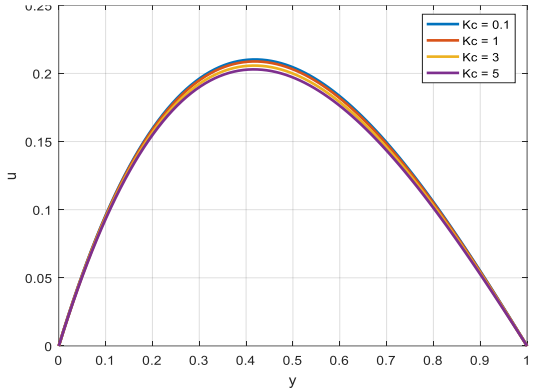

Figure 4.6: Velocity for different values of Kc

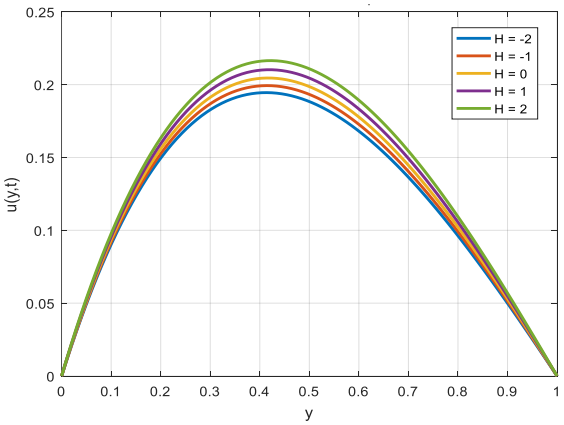

Figure 4.7: Velocity for different values of H

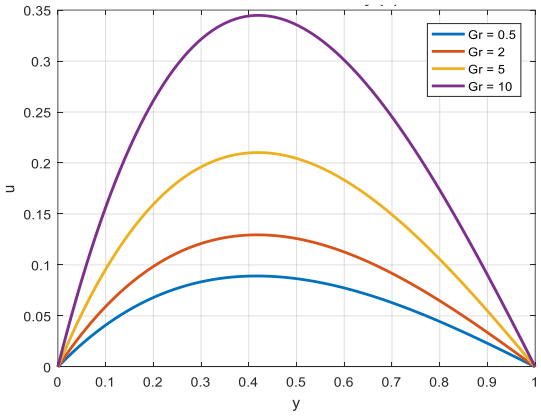

Figure 4.8: Velocity for different values of Gr

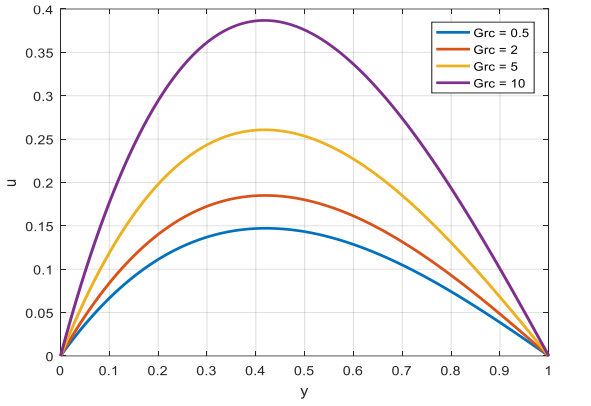

Figure 4.9: Velocity for different values of Grc

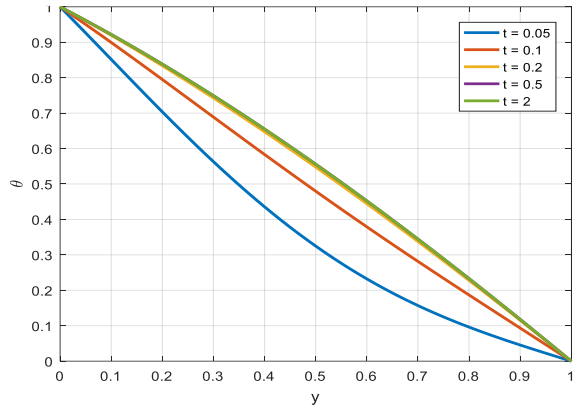

Figure 4.10: Temperature for different values of t

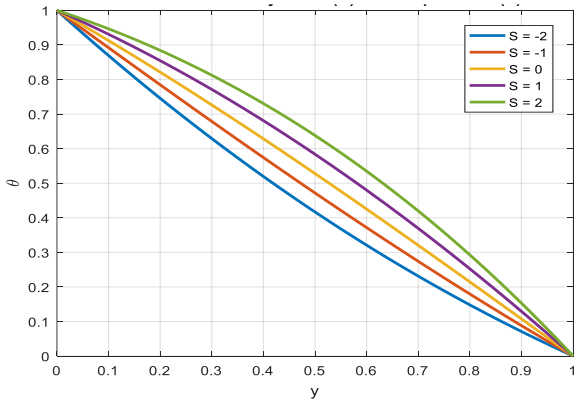

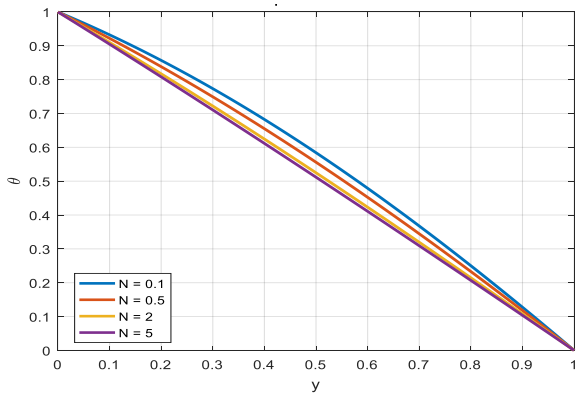

Figure 4.11: Temperature for different values of S

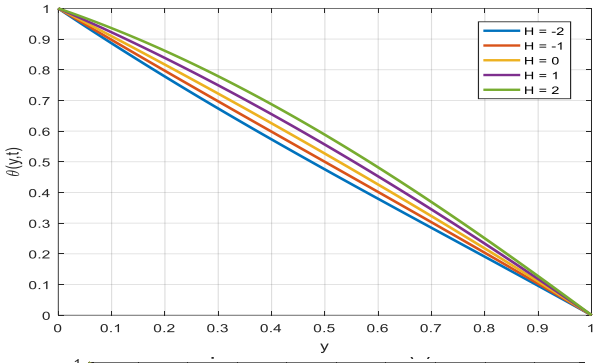

Figure 4.12: Temperature for different values of N

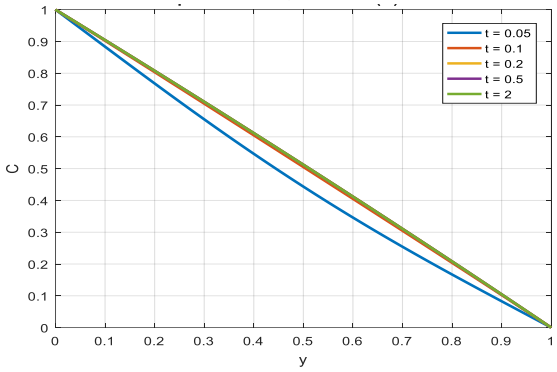

Figure 4.13: Temperature for different values of H

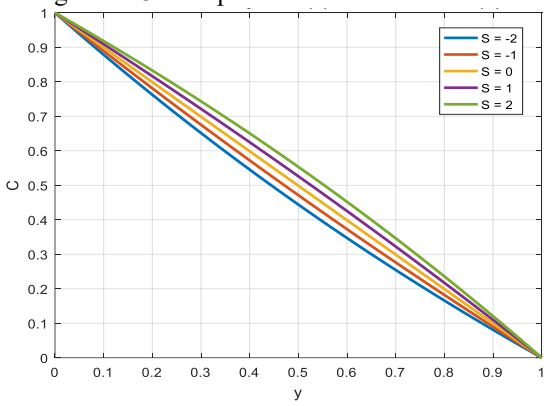

Figure 4.14: Concentration for different values of t

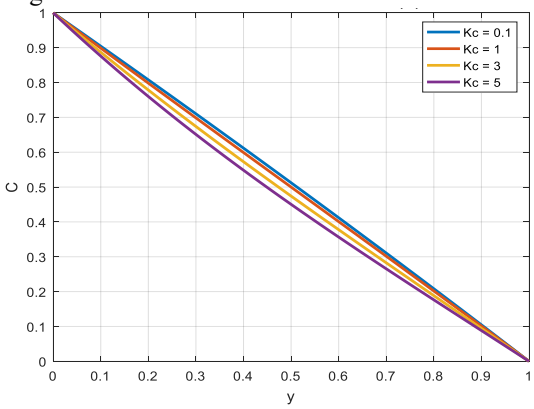

Figure 4.15: Concentration for different values of S

Figure 4.16: Concentration for different values of Kc

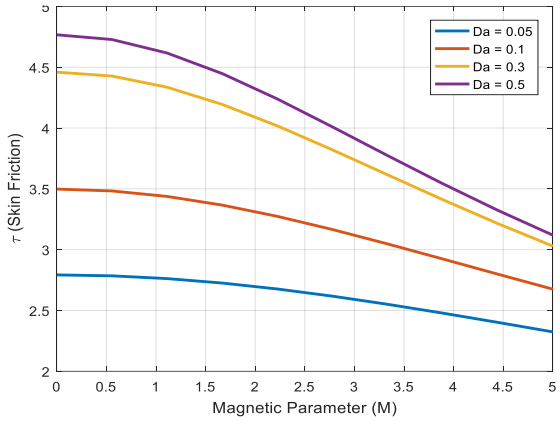

Figure 4.17: Skin friction against M varying Da

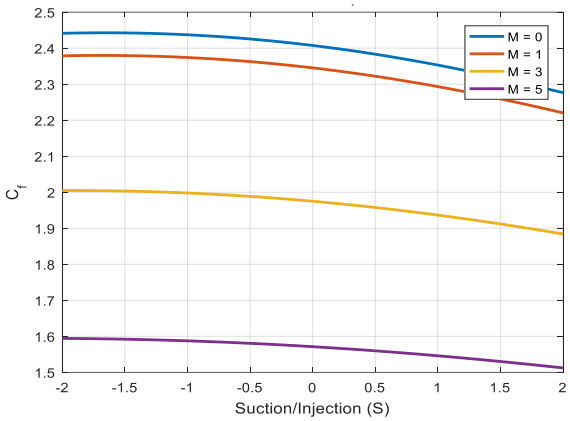

Figure 4.18: Skin friction against S varying M

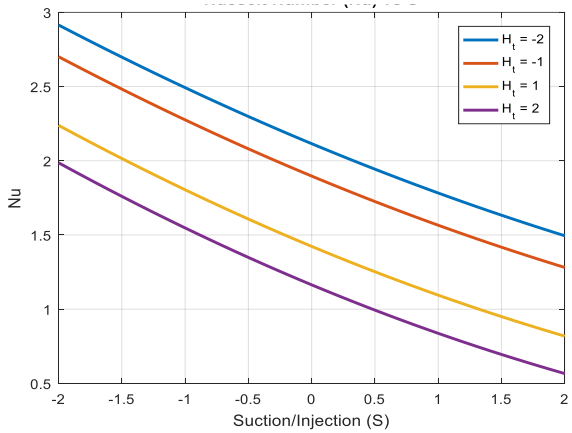

Figure 4.19: Nusselt Number against S varying H_t

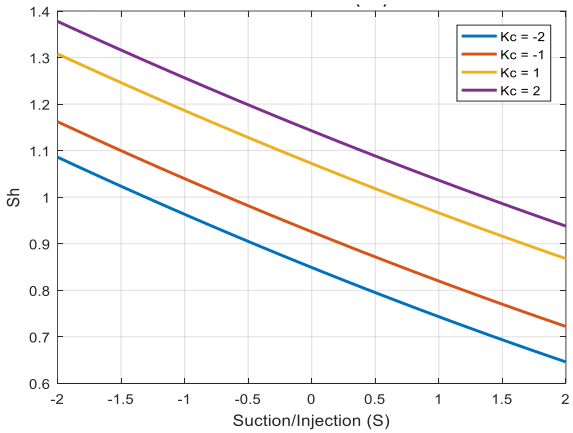

Figure 4.20: Sherwood number against S varying

4.2 DISCUSSION

Figure 4.1 illustrates the influence of time t on the velocity distribution of the Casson fluid within the vertical channel. It is observed that the velocity profile increases gradually as time progresses. At the initial stage of the motion, the fluid is almost stationary due to the imposed initial conditions, resulting in very small velocity values throughout the channel. As time increases, the momentum diffusion process becomes more pronounced and the fluid begins to accelerate under the combined influence of buoyancy forces associated with temperature and concentration gradients. This causes a progressive growth of the velocity boundary layer. The increasing velocity with time indicates that the flow gradually approaches a developed state as the transient effects diminish. Physically, this behaviour is expected because time allows the fluid particles to respond to the applied forces and transport mechanisms governing the system.

Figure 4.2 depicts the effect of the suction/injection parameter S on the velocity distribution across the channel. It is evident that increasing the suction parameter leads to a noticeable reduction in the velocity profile. Suction removes fluid particles from the boundary layer region, thereby reducing the thickness of the momentum boundary layer and suppressing fluid motion. This stabilizes the flow and results in a decrease in velocity magnitude throughout the channel. Conversely, when injection is present, additional fluid is introduced into the boundary layer which tends to enhance the flow velocity. The results clearly demonstrate that suction acts as a controlling mechanism that dampens the fluid motion, while injection tends to intensify it. From a physical standpoint, suction strengthens the adherence of the fluid to the wall surface, which increases the resistance to motion and reduces the overall velocity field.

Figure 4.3 shows the effect of the radiation parameter Nr on the velocity profile of the Casson fluid. It is observed that the velocity increases as the radiation parameter increases. Thermal radiation enhances the thermal energy within the fluid, which consequently raises the fluid temperature. The increase in temperature intensifies the buoyancy forces associated with the thermal Grashof number. As a result, the fluid particles experience an additional driving force that accelerates the motion of the fluid. This leads to a thicker velocity boundary layer and an increase in the velocity magnitude throughout the channel. The results therefore indicate that thermal radiation contributes significantly to the enhancement of fluid motion. This behaviour is physically reasonable because radiation acts as an additional mode of heat transfer, thereby increasing the energy available in the fluid and promoting stronger convective flow.

Figure 4.4 illustrates the influence of the magnetic parameter M^2 (Hartmann number) on the velocity distribution. The results indicate that the velocity decreases significantly with increasing values of M^2. This behaviour is attributed to the presence of a transverse magnetic field which generates a resistive force known as the Lorentz force. The Lorentz force acts in the opposite direction to the fluid motion and therefore suppresses the velocity of the electrically conducting Casson fluid. As the magnetic parameter increases, the strength of this electromagnetic force becomes stronger, which leads to greater resistance to the fluid flow. Consequently, the momentum boundary layer becomes thinner and the overall velocity profile decreases. This phenomenon is consistent with classical magnetohydrodynamic flow behaviour where magnetic fields are used to control or retard fluid motion in conducting fluids.

Figure 4.5 demonstrates the effect of the Darcy number Da on the velocity distribution. The Darcy number represents the permeability of the porous medium. It is observed that the velocity increases with increasing values of Da. When the Darcy number is small, the porous medium offers strong resistance to the fluid motion, which restricts the movement of fluid particles and results in lower velocity values. However, as the Darcy number increases, the permeability of the porous medium improves and the resistance to flow decreases. This allows the fluid to move more freely through the porous structure, leading to an increase in the velocity magnitude and a thicker momentum boundary layer. Therefore, the results suggest that highly permeable porous media facilitate fluid motion, while low permeability environments tend to suppress the velocity field.

Figure 4.6 presents the effect of the chemical reaction parameter Kc on the velocity profile. It is observed that the velocity decreases as the chemical reaction parameter increases. A stronger chemical reaction tends to reduce the concentration of the diffusing species within the fluid due to the consumption of reactants. Since the concentration difference contributes to the buoyancy force represented by the solutal Grashof number, a reduction in concentration weakens this buoyancy effect. Consequently, the driving force responsible for enhancing the fluid motion becomes weaker, resulting in a reduction in velocity. Furthermore, the presence of chemical reactions tends to stabilize the flow and reduce the thickness of the velocity boundary layer. Therefore, increasing the chemical reaction parameter leads to a suppression of the fluid motion within the channel.

Figure 4.7 illustrates the influence of the heat source parameter H on the velocity distribution. The results show that the velocity increases with increasing values of the heat source parameter. The presence of a heat source introduces additional thermal energy into the fluid system, which increases the fluid temperature. This rise in temperature enhances the thermal buoyancy force represented by the thermal Grashof number. As a result, the fluid experiences stronger upward motion due to the buoyancy-driven convection mechanism. Consequently, the velocity boundary layer thickness increases and the velocity magnitude becomes higher throughout the channel. The presence of internal heat generation therefore promotes fluid motion and intensifies convective heat transfer within the flow system.

Figure 4.8 shows the variation of velocity with the thermal Grashof number Gr. The results clearly indicate that the velocity profile increases significantly with increasing values of the thermal Grashof number. The thermal Grashof number represents the ratio of buoyancy forces to viscous forces in the fluid. When Gr increases, the buoyancy forces generated by temperature differences become stronger and dominate the viscous resistance within the fluid. This enhanced buoyancy effect accelerates the fluid particles and increases the velocity magnitude across the channel. Consequently, the velocity boundary layer becomes thicker as the thermal Grashof number increases. This behaviour confirms that thermal buoyancy plays a crucial role in driving the natural convection flow within the vertical channel.

Figure 4.9 illustrates the influence of the solutal Grashof number Grc on the velocity distribution. The results indicate that the velocity increases with increasing values of Grc. The solutal Grashof number represents the buoyancy force generated due to concentration differences within the fluid. When the concentration gradient becomes stronger, the density variation caused by mass diffusion enhances the buoyancy force acting on the fluid particles. This additional buoyancy force contributes to the acceleration of the fluid, thereby increasing the velocity magnitude. As a result, the momentum boundary layer becomes thicker and the fluid motion intensifies throughout the channel. This observation confirms that concentration-driven buoyancy significantly contributes to the overall fluid motion in combined heat and mass transfer problems.

Figure 4.10 shows the effect of time on the temperature distribution within the fluid. The results reveal that the temperature profile increases gradually as time increases. At the initial stage, the thermal boundary layer is very thin because the heat transfer process has just begun. However, as time progresses, thermal energy diffuses from the heated surface into the fluid region. This diffusion process causes the temperature of the fluid to increase and the thermal boundary layer to expand. The increase in temperature with time indicates that the system is evolving toward a steady thermal state where the heat transfer becomes more established. This behaviour is typical in transient heat transfer problems where time plays a significant role in the development of the temperature field.

Figure 4.11 presents the influence of the suction parameter on the temperature distribution. It is observed that the temperature profile decreases with increasing suction parameter. Suction removes heated fluid particles from the boundary layer region and replaces them with relatively cooler fluid from the outer region. This process reduces the thermal energy within the boundary layer and consequently lowers the temperature distribution. As a result, the thermal boundary layer thickness becomes thinner. Therefore, suction enhances the cooling effect within the flow system and reduces the temperature field. This behaviour indicates that suction can be effectively used as a mechanism to control heat transfer in thermal systems involving porous channels.

Figure 4.12 shows that the temperature increases significantly with increasing radiation parameter Nr. Thermal radiation contributes additional energy to the fluid through radiative heat transfer mechanisms. As the radiation parameter increases, more thermal energy is absorbed by the fluid, which raises the temperature distribution within the boundary layer. Consequently, the thermal boundary layer thickness increases and the temperature gradient near the wall decreases. This indicates that radiation plays a vital role in enhancing the thermal energy within the system, particularly in high temperature environments where radiative heat transfer becomes significant.

Figure 4.13 illustrates the effect of the heat source parameter on the temperature field. It is observed that the temperature increases with increasing values of H. Internal heat generation introduces additional thermal energy directly into the fluid domain, thereby increasing the overall temperature of the fluid. As a result, the thermal boundary layer becomes thicker and the temperature distribution across the channel rises. The presence of a heat source therefore intensifies the thermal energy of the system and significantly influences the heat transfer process.

Figure 4.14 depicts the effect of time on the concentration distribution. The concentration profile increases gradually as time progresses. At the beginning of the process, the concentration boundary layer is very thin because mass diffusion has not fully developed. However, as time increases, the diffusing species gradually penetrates deeper into the fluid, which increases the concentration levels across the channel. This leads to the development of a thicker

concentration boundary layer and a more uniform concentration distribution within the fluid.
Figure 4.15 shows that the concentration profile decreases with increasing suction parameter. Suction removes fluid particles containing the diffusing species from the boundary layer, thereby reducing the concentration level near the wall. This results in a thinner concentration boundary layer and a decrease in the overall concentration distribution within the fluid.
Figure 4.16 demonstrates that increasing the chemical reaction parameter significantly reduces the concentration distribution. Stronger chemical reactions consume the diffusing species within the fluid, thereby reducing the concentration level. This causes a decrease in the concentration boundary layer thickness and weakens the mass transfer process within the flow system.
Figure 4.17 shows the variation of the skin friction coefficient with the magnetic parameter for different values of the Darcy number. The results indicate that skin friction increases with increasing magnetic parameter. The presence of a stronger magnetic field increases the resistance to fluid motion, which results in higher shear stress at the wall surface. However, increasing the Darcy number tends to reduce the skin friction because higher permeability allows the fluid to flow more freely through the porous medium.
Figure 4.18 illustrates the variation of skin friction with suction parameter for different magnetic field strengths. The results indicate that skin friction increases with increasing suction parameter. Suction reduces the boundary layer thickness and increases the velocity gradient near the wall, which leads to higher shear stress and consequently higher skin friction.
Figure 4.19 shows the effect of suction parameter on the Nusselt number for different values of the heat source parameter. The Nusselt number increases with increasing suction because suction reduces the thermal boundary layer thickness and enhances the temperature gradient at the wall. However, increasing the heat source parameter tends to reduce the Nusselt number because internal heat generation reduces the temperature gradient near the wall surface.
Figure 4.20 presents the variation of the Sherwood number with suction parameter for different values of the chemical reaction parameter. The results indicate that the Sherwood number increases with increasing suction parameter because suction reduces the concentration boundary layer thickness and enhances the mass transfer rate. Furthermore, stronger chemical reactions increase the concentration gradient at the wall, which also contributes to higher Sherwood number values.

5. Conclusion

The study examines how flow and transport characteristics of Casson fluid in a vertical channel are affected by several governing parameters. Velocity increases with time, radiation parameter, heat source, Darcy number, and both thermal and solutal Grashof numbers due to enhanced driving forces. In contrast, it decreases with rising magnetic, suction, and chemical reaction parameters due to resistive forces. Temperature distribution rises with time, radiation, and heat source, but suction reduces it by removing heated fluid particles. Concentration similarly increases with time but decreases when suction and chemical reactions are present. Engineering metrics show that skin friction increases with magnetic field strength and suction, while it decreases with higher Darcy number. The Nusselt number rises with suction but falls with heat source, and the Sherwood number increases due to suction and chemical reaction, indicating improved mass transfer. The findings emphasize the critical role of heat absorption, viscous dissipation, and related parameters in influencing flow, heat, and mass transfer in Casson fluid systems, the result of katera and petal (2019) are obtain in the absent of injection and radiation and the present of heat generation.

REFERENCES

Abo-Dahab, S. M., Abdelhafez, M. A., Mebarek-Oudina, F., & Bilal, S. M. (2021). MHD Casson nanofluid flow over nonlinearly heated porous medium in presence of extending surface effect with suction/injection. *Indian Journal of Physics, 95*(12), 2703–2717. https://doi.org/10.1007/s12648-020-01923-z

Akbar, N., Hussain, S. M., & Khan, R. U. (2022). Numerical solution of Casson fluid flow under viscous dissipation and radiation phenomenon. *Journal of Applied Mathematics and Physics, 10*(2), 475–490.

https://doi.org/10.4236/jamp.2022.102036

Anwar, T., Kumam, P., & Watthayu, W. (2021). Unsteady MHD natural convection flow of Casson fluid incorporating thermal radiative flux and heat injection/suction mechanism under variable wall conditions. *Scientific Reports, 11*(1), 4275. https://doi.org/10.1038/s41598-021-83691-2

Awais, M., Raja, M. A. Z., Awan, S. E., Shoaib, M., & Ali, H. M. (2021). Heat and mass transfer phenomenon for the dynamics of Casson fluid through porous medium over shrinking wall subject to Lorentz force and heat source/sink. *Alexandria Engineering Journal, 60*(1), 1355–1363. https://doi.org/10.1016/j.aej.2020.10.056

Bathmanaban, P., Siva, E. P., Santra, S. S., Askar, S. S., Foul, A., & Nandi, S. (2024). Heat and mass transfer in double-diffusive mixed convection of Casson fluid: Biomedical applications. *Colloid and Polymer Science, 302*(10), 1635–1669. https://doi.org/10.1007/s00396-024-05310-6

Das, M., Mahato, R., & Nandkeolyar, R. (2015). Newtonian heating effect on unsteady hydromagnetic Casson fluid flow past a flat plate with heat and mass transfer. *Alexandria Engineering Journal, 54*(4), 871–879. https://doi.org/10.1016/j.aej.2015.07.007

Ilango, M. S., & Lakshminarayana, P. (2024). Induced magnetic field and Soret–Dufour effects on viscous dissipative Casson fluid flow through porous medium over a stretching sheet. *Journal of Thermal Analysis and Calorimetry, 149*(15), 8713–8727. https://doi.org/10.1007/s10973-024-13352-9

Kumar, V. V., Shekar, M. R., & Bejawada, S. G. (2023). Role of Soret and Dufour influence on unsteady MHD oscillatory Casson fluid flow on an inclined vertical porous plate in the existence of chemical reaction. *Journal of Advanced Research in Fluid Mechanics and Thermal Sciences, 110*(2), 157–175. https://doi.org/10.37934/arfmts.110.2.157175

Kumar, V. V., Shekar, M. R., & Bejawada, S. G. (2025). Thermo-diffusion and diffusion-thermo impacts on heat and mass transfer Casson fluid flow with porous medium in the presence of heat generation and radiation. *Partial Differential Equations in Applied Mathematics, 13*. https://doi.org/10.1016/j.padiff.2024.101039

Mangamma, I., Reddy, Y. D., Goud, B. S., Hendy, A. S., & Said, M. (2024). Soret and radiation influence on magneto Casson fluid flow over a non-linear inclined sheet in a Forchheimer porous medium with viscous dissipation. *Case Studies in Thermal Engineering, 64*. https://doi.org/10.1016/j.csite.2024.105463

Mythili, D., & Sivaraj, R. (2016). Influence of higher order chemical reaction and non-uniform heat source/sink on Casson fluid flow over a vertical cone and flat plate. *Journal of Molecular Liquids, 216*, 466–475. https://doi.org/10.1016/j.molliq.2016.01.072

Nihaal, K. M., Mahabaleshwar, U. S., Swaminathan, N., Laroze, D., & Pérez, L. M. (2025). Thermal transfer enhancement in a Casson-based hybrid nanofluid flow in a permeable wall jet with suction and injection.

Multiscale and Multidisciplinary Modeling, Experiments and Design, 8(3), 1–12.

Nisar, Z., Muhammad, K., Aldosari, F. M., & Elseesy, I. E. (2025). Peristaltic flow of MHD Casson nanofluid with heat source/sink and thermal radiation. *ZAMM – Journal of Applied Mathematics and Mechanics, 105*(1), e202300964. https://doi.org/10.1002/zamm.202300964

Ramzan, M., Shaheen, N., Chung, J. D., Kadry, S., Chu, Y. M., & Howari, F. (2021). Impact of Newtonian heating and Fourier and Fick's laws on a magnetohydrodynamic dusty Casson nanofluid flow with variable heat source/sink over a stretching cylinder. *Scientific Reports, 11*(1), 2357. https://doi.org/10.1038/s41598-021-81747-x

Reddy, N. A., & Janardhan, K. (2017). Soret and Dufour effects on MHD Casson fluid over a vertical plate in presence of chemical reaction and radiation. *International Journal of Current Research and Review, 9*(24), 55–61. https://doi.org/10.7324/IJCRR.2017.92411

Reddy, G. J., Raju, R. S., & Rao, J. A. (2018). Influence of viscous dissipation on unsteady MHD natural convective flow of Casson fluid over an oscillating vertical plate via FEM. *Ain Shams Engineering Journal, 9*(4), 1907–1915. https://doi.org/10.1016/j.asej.2016.10.012

Rehman, A. U., Jarad, F., & Riaz, M. B. (2024). A fractional study of MHD Casson fluid motion with thermal radiative flux and heat injection/suction mechanism under ramped wall condition: Application of Rabotnov exponential kernel. *Acta Mechanica et Automatica, 18*(1), 84–92. https://doi.org/10.2478/ama-2024-0011

Vinod, Y., Raghunatha, K. R., Nagappanavar, S. N., Nazarova, N., & Gupta, M. (2025). Boundary layer flow of a non-Newtonian fluid over an exponentially stretching sheet with the presence of a heat source/sink. *Partial Differential Equations in Applied Mathematics*. https://doi.org/10.1016/j.padiff.2025.101111